

**IMECE2010-38669**

**DYNAMIC MODELING AND FLUID-STRUCTURE INTERACTIVE ANALYSIS OF AN  
INNOVATIVE SELF-TUNING SHOCK ABSORBER FOR THE PROSTHESIS KNEE JOINT**

**Yen-Chieh Mao\***

Department of Mechanical Design Engineering, National Formosa  
University  
No. 64 Wen-Hua Rd., Hu-Wei Township, Yun-Lin County, 632 Taiwan  
R.O.C.

\*Corresponding author. EMail: [yjmau63@gmail.com](mailto:yjmau63@gmail.com)

**Wei-Chih Chang**

Department of Mechanical Design Engineering, National Formosa  
University  
No. 64 Wen-Hua Rd., Hu-Wei Township, Yun-Lin County, 632 Taiwan  
R.O.C.

**ABSTRACT**

The above-knee prosthesis, as a supplement of the lost biological leg, is supposed to provide equivalent or enhanced shock absorption capability and reduce the shock waves on the amputee body when walking and running. Prosthesis knee joint with a shock absorber is a feasible solution that efficiently absorbs the impact loads during each heel-strike. Conventional shock absorbers consist of springs and dampers with constant coefficients produce excessive rigid reactions when encountering impact forces, while unreasonable weak responses for gentle loads. This study proposes an innovative viscous damper design for the prosthesis knee joint which automatically and smoothly tunes the damping coefficient without any electronic components according to the input force velocities. High order differential system of the shock absorber is constructed and simulates the system dynamics during cyclic loads. The fluid-structure interactive finite element model for key components in the absorber is established in this study. Design parameters of the damper system under certain absorbing performance requirements are determined in this paper.

**INTRODUCTION**

The human locomotion system is subjected to repetitive

impact loads at heel strike, consisting of frequency spectra up to 100Hz during normal walking [1]. The shock force transfers through the foot, limb structure and up to the trunk, producing a considerable damage to human body and joints. The biologic shock absorbing structure in the musculoskeletal system provides viscoelastic mechanical behavior, which is relatively ineffective in withstanding sudden impulsive loads. This phenomenon is suggested as a primary etiological agent in some conditions, such as degenerative joint disease, prosthetic joint loosening, plantar fasciitis or muscle tears. Because foot loading and structure have a significant impact on the development of stress fractures, it is logical that shock-absorbing performance of prosthesis foot or leg can play an important role in the development, treatment and prevention of stress fractures [2].

The shock absorber is a key component in the prosthesis leg system. The spring and damping coefficients dominate a shock absorber's performances, which in terms affect the impact force absorption, releasing and contact condition between the foot and ground surface. This study focuses on the damping coefficient  $C$  of a shock absorber equipped in a prosthesis leg. The human body will experience an impact force if  $C$  is too large during a heel strike or falling onto the ground. However, the body will excessively lower down its altitude, reach its lower bound, hit the mechanical stopper and produce another impact force if  $C$  is too small. Therefore

appropriately selected  $C$  is critical in a shock absorption system.

Some research efforts focus on the suspension utilized with above-knee amputation proximal to the femoral condyles, including types of suction, silesian belt, and hip joint with pelvic band [4]. However shock absorption performances of these designs are limited to the space nearby the hip joint. A new class of power-harvesting prosthetic foot has been developed [5], as shown in Fig. 1, storing the wasted walking energy to work enhancing the power of ankle push-off. Test subjects spent 14% more energy walking in the energy-recycling artificial foot than they did walking naturally, representing a significant decrease from the 23% more energy they used in the conventional prosthetic foot. However, this kind of prosthesis needs an electric circuit, actuators and occupies considerable computations to deal with impact loads.



Fig. 1 Power-harvesting prosthetic foot.

Farber and Jacobson proposed a novel above-knee prosthesis design with an energy recovery system, which absorbs shocks during early stance and prevents impact from the anterior brim of the socket [8]. Johansson *et al.* give an evidence of variable-damping knee prostheses offer improved performance over mechanically passive prostheses for transfemoral amputees by comparing two variable-damping knees with the mechanically passive one [9]. Results show that the test user's metabolic rate with variable-damping knee prosthesis decreases by 3% to 5% compared with that of passive ones.

Considering the fluid dynamics, Mollica and Youcef-Toumi proposed a physical model for a high pressure monotube shock absorber to analyze the nonlinear dynamic behavior of these dampers [10]. Results explained that the frequency dependency of the hysteresis is produced by the interaction that at higher frequencies results in added phase loss due to the capacitive elements. Goncalves evaluated the dynamic response of different semi-active control policies over a magneto-rheological damper as tested on a single suspension quarter-car system [11]. Duym *et al.* presented an overview of shock absorber models [12]. A nonparametric model, models the damper force as a function of both velocity and acceleration, based on an alternative restoring force considerably reduces the residual error. Bathe *et al.* presented advances in capabilities for the analysis of fluid flows with structural interactions [13]. An arbitrary Lagrangian-Eulerian formulation is used to solve for the fluid response with structural interface and free surface conditions.

## THE PROPOSED DESIGN

### Overview

The most significant problem of a suspended prosthesis leg is their tendency to dissipate propelling energy through the shock absorber. As the amputee imparts force into the prosthesis leg, the parallel vector (coincide with the shock absorber axis) component causes the prosthesis to bob on its suspension. This undesirable shock absorption movement dissipates a significant percentage of the imparted propelling energy and can reduce the amputee's overall locomotive efficiency.

This research proposes an innovative self-tuning damper of a shock absorber for above-knee prostheses equipped in the tibia section, as shown in Fig. 2.

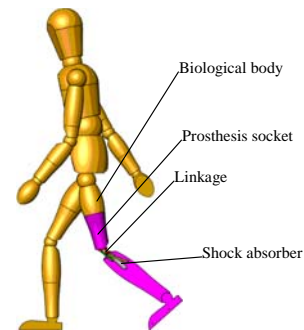


Fig. 2 The proposed shock absorber in the prosthesis.

### Apparatus Configuration and Operations

Figure 3 sketches out the overall configuration of the proposed design, comprising of the key components in the prosthesis shock absorber. The damping stator is fixed in the upper tube. The main piston, synchronally moving with the lower tube, impels and draws the oil in the lower chamber. The fluid, passing through the orifices inside the damping stator, flows back and forth between the upper and lower chambers. The separation film keeps the air in the top chamber from mixing with oil in the upper chamber.

The fluid circuit inside the damping stator is shown in Fig. 4. When the amputee is during the gait phase of heel-strike, an impact force drives the main piston toward the upper side of the damper. The high-pressure fluid in the lower chamber is impelled into the upper chamber, achieving the pressure-release process.

Take the contraction spool valve for illustration. The fluid pushes the contraction spool valve against the spring at this moment. The valve keeps closed before the lower chamber pressure rises up to a first predetermined level, functioning as an automatic locking-out capability. The valve opens an equivalent orifice and allows the fluid flow through the passage if the pressure is high enough to balance or surpass the spring force. The damping coefficient is decreased as the equivalent orifice area is increased, achieving an automatic tuning

function. The contraction check valve opens and allows a maximum flow rate to pass through when the lower chamber pressure exceeds a second predetermined value, achieving the rapid-releasing function.

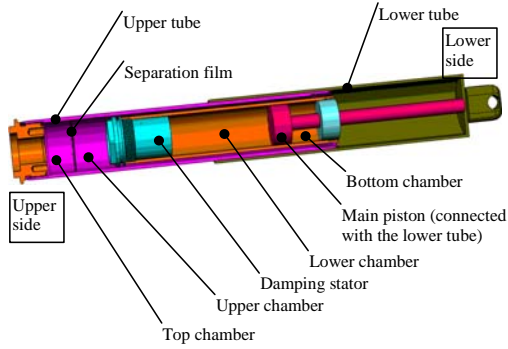


Fig. 3 The overall sectional view of the proposed design.

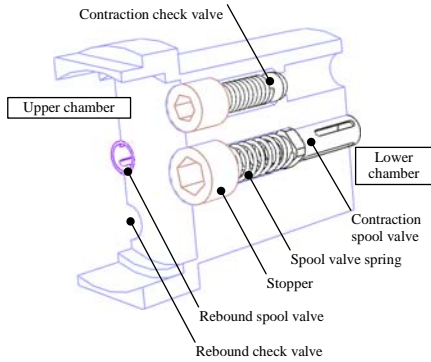


Fig. 4 Fluid circuits inside the damping stator.

### THE SIMPLIFIED FSI MODEL

The shock absorber mechanical structure in this design produces small strains while large displacements during cyclic loads of amputee gaits. The mechanical and fluidic components deliver various forces among their contact interfaces and produce unneglectable displacements and force changes on these interfaces, constructing a fluid-structure interaction (FSI) problem. The top pneumatic chamber represents a nonlinear spring to support the amputee body weight. The spool valve effective orifice area correlates with the transient pressure difference between the lower and upper chambers, characterizing a nonlinear damping property as well. To deal with the nonlinear dynamic FSI problem, the finite element program ADINA by ADINA R&D Inc. is chosen in this study. The system is illustrated in Fig. 5, which demonstrates a simplified axial symmetrical configuration.

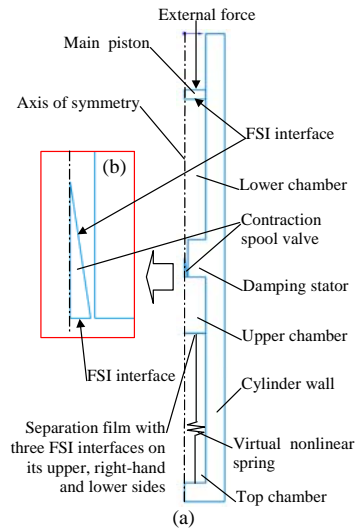


Fig. 5 System model constructed in ADINA program.

This model eliminates check valves since they are always inactivated in the normal pressure difference levels. Only the spool valve of contraction side is simulated in this model because of the rebound flow similarity. External force is set to be sinusoidal 20N in  $\pi$  rad/s to reduce the turbulence in the field; friction forces are not considered in this simulation. The pneumatic air spring by the top chamber is replaced with an equivalent virtual nonlinear mechanical spring, reducing the complexity and number of element nodes in this model. Physical parameters are listed in Table 1, which are also employed in the theoretical model in the later section. Simulation results are demonstrated in Fig. 6.

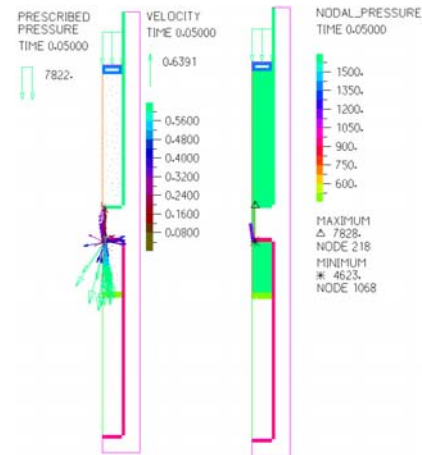


Fig. 6 The simplified FSI model of the proposed design.

It is observed that the velocity and pressure field nearby the contraction spool valve opening is greatly changed as the external force rises, enlarging the effective orifice area. This phenomenon is verified to reduce the damping coefficient in the theoretical section.

## THEORETICAL MODELLING OF THE DYNAMICS

The physical model employed in the theoretical analysis is defined in Fig. 7. Initial volume of the top, upper, lower and bottom chambers are  $V_{t0}$ ,  $V_{u0}$ ,  $V_{l0}$  and  $V_{b0}$ , respectively. The time-derivative of the propelling force  $F_m$  is modeled as a cosine wave with the amplitude of  $F_0$ :

$$\dot{F}_m = F_0 \cos(\omega t + \phi)$$

where  $\omega$  is a constant angular velocity,  $\phi$  denotes the initial angular position of the driving force. The resultant force pushes the main piston upward to a certain position  $x_m$ .

$$m_m \ddot{x}_m + C_m \dot{x}_m + k_m x_m = F_m - P_l A_{m1} + P_b A_{m2} + P_a A_{m3} - m_m g$$

where  $C_m$  is the damping coefficient caused by friction;  $k_m$  denotes the main spring in the shock absorber;  $P_a$  is the atmosphere of  $1.0134 \times 10^5$  Pa;  $g$  represents the gravity.

The spool valve movements induce the damping characteristics of the proposed design, as defined in Fig. 8. Contraction and rebound spool valves work at the opposite sides in the damping stator, and have the similar operating conditions. They slide in the valve tunnels according to the pressures in the lower and upper chambers.

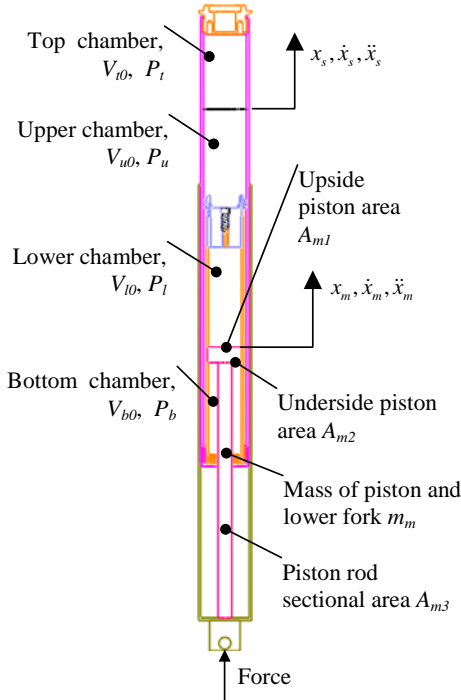


Fig. 7 Mathematical model of the damper.

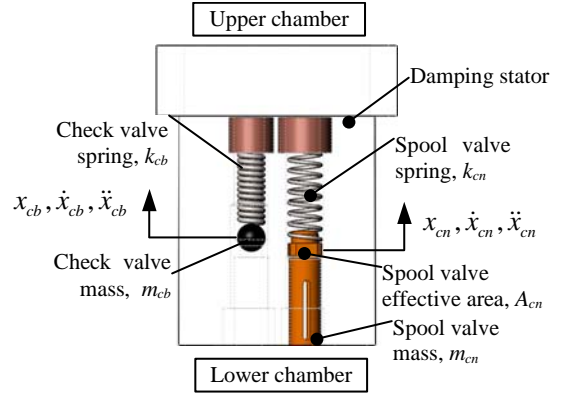


Fig. 8 Model of the contraction valves in the damping stator.

For the contraction and rebound spool valves, respectively:

$$m_{cn} \ddot{x}_{cn} + C_{cn} \dot{x}_{cn} + k_{cn} x_{cn} = P_l A_{cn} - P_u A_{cn} - m_{cn} g$$

$$m_{rn} \ddot{x}_{rn} + C_{rn} \dot{x}_{rn} + k_{rn} x_{rn} = -P_l A_{rn} + P_u A_{rn} + m_{rn} g$$

For the contraction and rebound check valves, respectively:

$$m_{cb} \ddot{x}_{cb} + C_{cb} \dot{x}_{cb} + k_{cb} x_{cb} = P_l A_{cb} - P_u A_{cb} + m_{cb} g$$

$$m_{rb} \ddot{x}_{rb} + C_{rb} \dot{x}_{rb} + k_{rb} x_{rb} = -P_l A_{rb} + P_u A_{rb} - m_{rb} g$$

where the positive directions of  $x_{rn}$  and  $x_{rb}$  are toward the ground.

The separation film is modeled as a piston with an extremely small mass  $m_s$ , and frictionless with the cylinder wall. The pressure difference between the upper and top chambers impels its movement:

$$m_s \ddot{x}_s + C_s \dot{x}_s = P_u A_s - P_t A_s - m_s g$$

The bottom chamber is initially filled with air of 1 atm. The pressure change rate varies with the main piston position and velocity:

$$\dot{P}_b = \gamma \frac{-P_b A_{m2} \dot{x}_m}{V_{b0} + A_{m2} x_m}$$

where  $\gamma$  is the specific heat ratio for air, and is selected as 1.4 in this simulation [14].

Pressure derivatives relate to the lower and upper chamber volumes, and the fluid flow rates between these chambers are:

$$\dot{P}_l = \beta \frac{A_{m1} \dot{x}_m - Q_1 + Q_3}{V_{l0} - A_{m1} x_m}; \dot{P}_u = \beta \frac{-A_s \dot{x}_s + Q_1 - Q_3}{V_{u0} + A_s x_s}$$

where  $\beta$  denotes the bulk modulus of the damping fluid, and has a value of  $1.52 \times 10^9$  N/m<sup>2</sup> for petroleum fluids [15];  $Q_1$ ,  $Q_3$  are the flow rates from lower to upper chamber, and that from upper to lower chamber, respectively:

$$Q_1 = C_{d1}A_1\sqrt{\frac{2(P_l - P_u)}{\rho}}; Q_3 = C_{d1}A_3\sqrt{\frac{2(P_u - P_l)}{\rho}}$$

where  $C_{d1}$  is the discharge coefficient of 0.7 in this study, which is sufficient for design purpose [16].

Pressure change rate in the top chamber can be defined as:

$$\dot{P}_t = \gamma \frac{P_t A_s \dot{x}_s}{V_{t0} - A_s x_s}$$

The entire model can be expressed using the previous derivations. These formulae represent a 15<sup>th</sup> order dynamic nonlinear system. The system outputs, the position  $x_m$  and velocity  $\dot{x}_m$  of the main piston, are of interest to this study.

## SIMULATION AND DISCUSSION

The frictional forces between pistons and cylinders are neglected. Damping coefficient due to the friction is modeled but set to be zero in this study.

The dimensions and masses involved in this simulation are evaluated from the CAD system. The complete parameter list is collected in Table 1. The Runge-Kutta method is employed to solve these ODEs [17]. Sampling time during the simulation is  $6.9444 \times 10^{-4}$ s, attentively tracking the dynamics with 720 data points per round in the 60 rpm cycles. Deformation of structures is not considered in this model.

The simulation result is shown in Fig. 9. Various quantities are normalized and combined in the same plot for the convenience of comparison. Refer to subplot (a),  $F_m$  indicates the sinusoidal reacting force from the ground to impel the main piston, having the maximum value of 786.51N. The main piston starts to oscillate with the input force after a slight delay of 0.03s, caused by the throttling effect of the spool valves. The maximum value of the main piston displacement is  $9.65 \times 10^{-3}$  m. The separation film coincides with main piston's normalized oscillation approximately with a displacement of  $6.32 \times 10^{-3}$  m, and it does not go through excessive negative value due to the upper chamber pressure.

TABLE 1 PARAMETERS AND VALUES EMPLOYED IN THIS STUDY.

Category	Object	Nomen.	Value
Mass of...(kg)	main piston	$m_m$	0.2363
	separation film	$m_s$	1.0000e-3
	contraction spool valve	$m_{cn}$	1.4400e-4
	rebound spool valve	$m_{rn}$	
	contraction check valve	$m_{cb}$	2.5460e-4
	Rebound check valve	$m_{rb}$	
Sectional area of...(m <sup>2</sup> )	upside main piston	$A_{m1}$	3.8708e-4
	bottom side main piston	$A_{m2}$	3.3681e-4
	main piston rod	$A_{m3}$	5.0265e-5

Category	Object	Nomen.	Value
	contraction spool valve (effective)	$A_{cn}$	1.0179e-5
	rebound spool valve (effective)	$A_{rn}$	
	separation film	$A_s$	5.9188e-4
Initial volume of...(m <sup>3</sup> )	bottom chamber	$V_{b0}$	1.6841e-5
	lower chamber	$V_{l0}$	1.9354e-5
	upper chamber	$V_{u0}$	1.4797e-5
	top chamber	$V_{t0}$	
Initial pressure in...(Pa)	bottom chamber	$P_{b0}$	1.0134e5
	lower chamber	$P_{l0}$	
	upper chamber	$P_{u0}$	
	top chamber	$P_{t0}$	
Spring constant of...(N/m)	main spring	$k_m$	78480
	contraction spool valve	$k_{cn}$	2036.6
	rebound spool valve	$k_{rn}$	1018.3
	contraction check valve	$k_{cb}$	3054.8
	rebound check valve	$k_{rb}$	
Bulk modulus (N/m <sup>2</sup> )		$\beta$	1.4911e9
Specific heat ratio		$\gamma$	1.4
Rotational speed of driving force (rad/s)		$w$	6.2832
Reacting force (from ground) amplitude (N)		$F_0$	784.8
Discharge coefficient of spool valves		$C_{d1}$	0.7

Pressure variations in the chambers are shown in subplot (b). The bottom chamber pressure starts to decrease since the main piston moves upward, and to increase when the main piston moves downward. The lower chamber pressure increases rapidly and rises to its maximum value  $2.59 \times 10^5$ Pa. Pressures in the upper and top chambers approximate with each other since there is no resistance on the separation film, valuing about  $1.51 \times 10^5$ Pa.

The force ( $F_m$ ) versus main piston displacement/velocity (D/V) plot is given in subplot (c). The  $F_m$ -D curve can be ignored since the proposed fluid-mechanical design is a velocity-sensitive fluid structure and irrelevant to the piston displacement. The maximal absolute value of force occurs when displacement is zero, since the piston reaches its maximal velocity when it passes the neutral position. The top-right corner of the  $F_m$ -V curve represents this phenomenon, saying the maximum velocity is  $6.19 \times 10^{-2}$ m/s. The damper shows a rigid-style shock absorber when the normalized velocity is below about 0.4, whereas it shifts to a soft-style suspension when velocity is above 0.8. This curve is more preferable for amputees because it reveals a rigid low-speed damping for a good yet firm controlled feeling, and a soft high-speed damping for a more comfortable walking on heel strikes or jumping.

Subplot (d) is generated from piston velocity with respect to  $F_m / \dot{x}_m$ , which represents the equivalent damping coefficient. Data points nearby zero velocity imply the mathematical transient state of the dynamic system, feasible to be disregarded in this study. However, the remaining portion of the curve shows a downside tendency approaching to zero coefficients as the piston velocity increases, achieving a different style against the constant-damping traditional shock absorber.

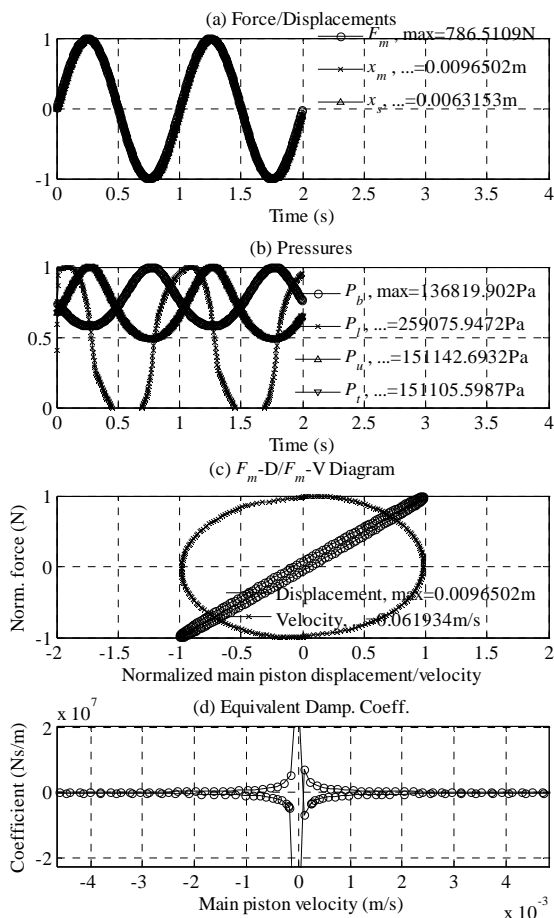


Fig. 9 Simulation results of the proposed shock absorber.

## CONCLUSION

This research proposes an innovative fluid shock absorber design equipped in an above-knee prosthesis. A simplified dynamic nonlinear finite element model with fluid-structure interaction interfaces is established and obtained the qualitative operation performance of the proposed design. This study constructed a theoretical high-order nonlinear system dynamic model. The simulation result explains that the proposed damper

in the shock absorber appears to be firmer when it run in a smooth loading condition, the amputee is propelling hard, because the input velocity of the force is relative small. On the other hand, the damper becomes softer when the amputee encounters relative large forces. More important, the switching processes are automatically achieved without any manual or electric operation. This study will enhance the FSI model capable of transient analysis to virtually confirm the theoretical model. It is necessary to construct a dynamic test rig to experimentally verify the shock absorber prototype.

## ACKNOWLEDGMENT

This work was supported by National Science Council in Taiwan R.O.C. under the project number NSC 98-2221-E-150-023. The authors would like to express their appreciates to Dr. Shen-Yeh Chen in FEA-Opt Technology Inc. for his technology support in ADINA software operations.

## REFERENCES

- [1] Y. Folman, J. Wosk, A. Voloshin, and S. Liberty, "Cyclic impacts on heel strike: a possible biomechanical factor in the etiology of degenerative disease of the human locomotor system." *Archives of Orthopaedic and Trauma Surgery*, Vol. 104, No. 6, 1986, pp. 363-365.
- [2] C. Frey, "Footwear and stress fractures," *Clinics in Sports Medicine*, Vol. 16, No. 2, 1997, pp. 249-257.
- [3] M. R. Pitkin, "Mechanical outcomes of a rolling-joint prosthetic foot and its performance in the dorsiflexion phase of transtibial amputee gait," *Journal of Prosthetics and Orthotics*, Vol. 7, No. 4, 1995, pp. 114-123.
- [4] C. J. Dietzen, J. Harshberger, and R. D. Pidikiti, "Suction sock suspension for above-knee prostheses," *Journal of Prosthetics and Orthotics*, Vol. 3, No. 2, 1991, pp. 90-93.
- [5] Donelan J. M., Li Q., Naing V., Hoffer J. A., Weber D. J. and Kuo A. D., 2008, "Biomechanical energy harvesting: generating electricity during walking with minimal user effort," *Science*, Vol. 319, pp. 807-810.
- [6] A. E. Barr, K. L. Siegel, J. V. Danoff, C.L. McGawey III, A. Tomasko, I. Sable, S.J. Stanhope, "Biomechanical comparison of the energy-storing capabilities of SACH and Carbon Copy 11 prosthetic feet during the stance phase of gait in a person with below-knee amputation," *Physical Therapy*, Vol. 72, No. 5, 1992, pp. 344-354.
- [7] K. Bharadwaj and T. G. Sugar, "Design of a robotic gait trainer using spring over muscle actuators for ankle stroke rehabilitation," *Journal of Biomechanical Engineering*, Vol. 127, 2005, pp. 1009-1013.
- [8] B. S. Farber, J. S. Jacobson, "An above-knee prosthesis with a system of energy recovery: a technical note,"

*Journal of Rehabilitation Research and Development*, Vol. 32, No. 4, 1995, pp. 337-348.

- [9] J. L. Johansson, D. M. Sherrill, P. O. Riley, P. Bonato and H. Herr, "A clinical comparison of variable-damping and mechanically passive prosthetic knee devices," *American Journal of Physical Medicine Rehabilitation*, Vol. 84, 2005, pp. 563-575.
- [10] R. Mollica & K. Youcef-Toumi, "A nonlinear dynamic model of a monotube shock absorber." *Proceedings of American Control Conference*, Albuquerque, NM, USA, 1997, 704-708.
- [11] F. D. Goncalves, *Dynamic analysis of semi-active control techniques for vehicle applications*, Master of Science in Mechanical Engineering, Virginia Polytechnic Institute and State University, 2001.
- [12] S. Duym, R. Stiens & K. Reybrouck, "Evaluation of shock absorber models," *Vehicle System Dynamics*, Vol. 27, 1997, pp. 109- 127.
- [13] K. J. Bathe, H. Zhang & S. Ji, "Finite element analysis of fluid flows fully coupled with structural interactions," *Computers & Structures*, Vol. 72, No. 1-3, 1999, 1-16.
- [14] E. C. Yeh, S. H. Lu, T. W. Yang & S. S. Hwang, "Dynamic analysis of a double tube shock absorber for robust design," *JSME International Journal Series C.*, Vol. 40, No. 2, 1997, 335-345.
- [15] R. H. Warring, *Hydraulic handbook*, Surrey, England: Trade & Technical Press Ltd., 1983.
- [16] H. E. Merritt, *Hydraulic control systems*, New York: John Wiley & Sons Inc., 1967.
- [17] G. Lindfield & J. Penny, *Numerical methods using MATLAB*, Prentice Hall International, 2001.